

# The distribution of stars near the super-massive black hole in the Galactic Center

Tal Alexander

Institute for Advanced Study, Olden Lane, Princeton, NJ 08540

## ABSTRACT

We analyze three sets of infrared star counts in the inner  $\sim 0.5$  pc of the Galactic Center. We perform statistical tests on the star counts and model in detail the extinction field and the effects of dwarf-giant collisions on the luminosity function. We find that both the star counts and the depletion of the brightest stars in the inner  $\sim 0.05$  pc can be explained by a  $n \propto r^{-\alpha}$  stellar cusp with  $\alpha$  in the range  $3/2$  to  $7/4$ , in which the envelopes of the brightest giants are destroyed by stellar collisions. Such a cusp is consistent with the Bahcall-Wolf solution for the distribution of stars that have undergone two-body relaxation around a black hole. We show that systematic uncertainties due to variable extinction and unrelaxed stars are probably small, but deeper star counts are required to confirm these results. We estimate that the tidal disruption rate of cusp stars by the black hole is  $\text{few} \times 10^{-5} \text{ yr}^{-1}$ .

*Subject headings:* Galaxy: center — Galaxy: kinematics and dynamics — Galaxy: stellar content — infrared: stars

## 1. Introduction

The Galactic Center (GC) offers a unique opportunity to study the dynamical effects of a super-massive black hole (BH) on the stellar population in its immediate vicinity. Dynamical models of the evolution of such a system generically predict the formation of a *stellar cusp* with a characteristic slope that reflects its formation history (Bahcall & Wolf 1976, 1977; Young 1980; Lee & Goodman 1989; Quinlan, Hernquist & Sigurdsson 1995). Although the existence of super-massive BHs in the center of normal galaxies now appears to be the rule rather than the exception (Magorrian et al. 1998), the observed central light distributions do not seem to be correlated with the mass of the central black hole (Kormendy & Richstone 1995; but see Magorrian et al. 1998). It appears that even on the smallest resolved scales of about  $0.1''$ , the light distribution still reflects the overall galactic dynamics, and that the effects of the BH on the spatial distribution of the stars may be confined to yet smaller scales. Even with better resolution, it will be very hard to observe individual stars in the dense galactic cores, and the properties

of the stellar population will have to be inferred from the projected integrated light, which is completely dominated by giants and supergiants. These rare stars may not be representative of the general stellar population. Furthermore, their light-emitting envelopes could be affected by various processes in the extreme environment inside a BH cusp. The situation is further complicated by the fact that galactic centers often display cusps in the light distribution on scales that are much too large to be related to the presence of a super-massive BH in the core. Obviously, other dynamical processes can also give rise to stellar cusps, so it is not possible to claim that a central stellar cusp *must* be related to the presence of a BH (Phinney 1989).

This is to be contrasted with the situation in the GC, where precise measurements of the apparent motions and radial velocities of individual stars have already made it possible to weigh the central BH dynamically, independently of the light distribution (Genzel et al. 1997; Ghez et al. 1998). This makes it legitimate to interpret the stellar distribution very near the center in the context of BH formation scenarios. These observations also yielded deep infrared star counts, which extend the stellar census to stars far less luminous and much more numerous than supergiants. However, the step from the observed number counts to the actual stellar distribution is far from trivial. Observations show that the stellar population of GC is a mixture of old and young stars, which are probably the products of episodic star-formation throughout the GC history (Genzel, Hollenbach & Townes 1994; Serabyn & Morris 1996). Some of the young and very luminous stars are not dynamically relaxed (Krabbe et al. 1995; Genzel et al. 1996). Spatial variations in the spectral properties of the stellar population (Sellgren et al. 1990; Krabbe et al. 1995; Genzel et al. 1996), and possible spatial gradients in the extinction (Blum et al. 1996; Davidge 1998), could further complicate the interpretation of the star counts. The necessary first step towards testing dynamical models in the inner GC is to establish what is the stellar distribution there.

The evidence for a stellar cusp within the cusp radius of the GC (roughly, the radius enclosing a stellar mass comparable to the BH mass, which is  $\sim 3$  pc in the GC) has so far been inconclusive or negative. The mass models that are currently adopted in stellar proper motion studies of the GC do not have an inner stellar cusp, but assume a smoothed isothermal distribution with a core radius of 0.4 pc ( $1'' = 0.04$  pc in the GC for a solar galactocentric distance of 8 kpc (Carney et al. 1995). In this work we re-examine the question of whether there is a stellar cusp in the inner  $10''$  of the GC.

This study is motivated by several recent developments. Progress in extending infrared observations of the GC to fainter magnitudes and higher angular resolutions (Genzel et al. 1997; Ghez et al. 1998) and to larger samples with multi-color information (Blum et al. 1996; Davidge et al. 1997; Davidge 1998) yielded a wealth of information on the distribution of stars in the GC. In addition, these deep infrared counts in the GC, together with infrared and optical star counts in Baade’s window (Tiede et al. 1995; Holtzman et al. 1998), now make it possible to reliably model the infrared stellar luminosity function in the GC over a large luminosity range (Alexander & Sternberg 1999). However, the high angular resolution studies are primarily focused on tracking stellar proper motions for weighing the BH, while the multi-color studies are focused on studying

the spectral properties of the stellar population. Consequently, the star counts, which are a by-product of these studies, have not yet been analyzed in detail, and the additional information supplied by the luminosity function has not been taken into account. Finally, recent high resolution deep imaging of the central few arcseconds revealed an apparent over-density of faint stars in the inner  $1''$  relative to the immediate surroundings, the so-called “Sgr A\* cluster” (Genzel et al. 1997; Ghez et al. 1998). This raises the question whether a distinct stellar cluster with an atypically faint stellar population could have possibly formed in the inner  $1''$  or else migrated there from farther away.

In this study we analyze the observed stellar distribution in three published data sets (§2.3): Keck data from Ghez et al. (1998), OSIRIS data from Blum et al. (1996) and SHARP+3D data from Genzel et al. (1996) and Eckart & Genzel (1997). As we will argue below, these data point to a simpler explanation for the Sgr A\* cluster, namely that it is the tip of an underlying stellar cusp that smoothly rises throughout the inner  $10''$ , and that the absence of luminous stars there is due to a combination of envelope-destroying stellar collisions and projection effects rather than an intrinsic change in the properties of the stellar population. We will further show that the shape of the cusp agrees with that predicted by the Bahcall-Wolf solution for the distribution of intermediate mass stars in a multi-mass system that has undergone two-body relaxation around a BH (Bahcall & Wolf 1976, 1977; Murphy, Cohn & Durisen 1991), as appears to be the case in the inner GC.

This paper is organized as follows. In §2 we describe the relevant properties of stars in the GC and present the data that are used in our analysis. In §3 we describe the stellar density distributions that we use to model the data and present the results of the statistical analysis of the counts. Some anomalies in the counts are further discussed in Appendix A. In §4 we investigate the effects of extinction on the star counts. Readers who are mainly interested in the dynamical results of this work may prefer to skip this section and proceed to §5, where we discuss the effects of stellar collisions on the depletion of the brightest stars. The orbitally-averaged collision rate is derived in Appendix B. We discuss the results in §6 and summarize our conclusions in §7.

## 2. Stars in the Galactic Center

### 2.1. The stellar population and stellar distribution

The stellar population in the GC is a mixture of old Galactic Bulge stars and younger stars that were produced in various star-formation episodes during the lifetime of the Galaxy (Genzel, Hollenbach & Townes 1994; Serabyn & Morris 1996). About 80% of the stars observed in the central parsec down to  $K = 14.5^m$  are identified as late-type giants and supergiants by their pronounced CO absorption. Late-type stars at the magnitude range  $11^m \lesssim K \lesssim 14.5^m$  are K and M giants, which correspond to a mass range of  $1-7M_\odot$  and ages  $> \text{few} \times 10^9$  yr. Late-type stars at the magnitude range  $9^m \lesssim K \lesssim 12^m$  are probably asymptotic giant branch (AGB) stars

in the mass range  $2\text{--}8M_{\odot}$  and ages of  $1\text{--}\text{few} \times 10^9$  yr. The most luminous late-type star, IRS7 ( $K = 6.5^{\text{m}}$ ), is a massive  $15\text{--}25M_{\odot}$  supergiant with an age of no more than  $10^7$  yr. The late-type giants are dynamically relaxed and follow the galactic rotation (Genzel et al. 1996).

The remaining  $\sim 20\%$  of the  $K < 14.5^{\text{m}}$  stars in the central parsec appear to be recently formed stars, either exhibiting strong HeI/HI emission or a steep featureless reddened continuum (Krabbe et al. 1995; Genzel et al. 1996). Two extended red objects, which may be recently formed stars still embedded in a dust shell, are also observed (Ott, Eckart & Genzel 1998). The HeI/HI stars are massive, hot and very luminous stars with huge mass loss rates, which are probably undergoing a short lived phase lasting less than  $10^5$  yr, on their way to becoming classical Wolf-Rayet stars. In this case, their progenitors must be  $\gtrsim 20M_{\odot}$  stars with main-sequence lifetimes shorter than  $10^7$  yr. The  $\sim 20$  HeI/HI stars in the inner few arcseconds supply more than 50% of the total  $2\mu\text{m}$  flux there. The fainter stars with the featureless reddened continua could be main-sequence O stars. The four stars in the Sgr A\* cluster (inner  $1''$ ) for which spectra were obtained appear to be such early-type stars (Genzel et al. 1997). Krabbe et al. (1995) modeled the HeI/HI stars and the late-type supergiants in the central parsec by a  $3000M_{\odot}$  starburst that occurred between 3 and  $8 \times 10^6$  yr ago. This is a very small fraction of the total stellar mass that is enclosed in the central parsec,  $\sim 1.5 \times 10^6 M_{\odot}$ . These recently formed stars are not dynamically relaxed, as is demonstrated by the radial velocity field of the HeI/HI stars in the inner  $\sim 10''$ , which clearly indicates that the stars are counter-rotating at a constant rotation velocity  $v_{\text{rot}} = 120 \text{ km s}^{-1}$  with respect to the galactic rotation of  $v_{\text{rot}} = 24 \text{ km s}^{-1}$ . There are additional indications that the stellar population varies with position and is not quite well-mixed. The depth of the CO absorption feature in the integrated light decreases in the inner  $\sim 10''$  (Sellgren et al. 1990). This is probably due to the joint effects of a depletion of the luminous ( $K < 10.5^{\text{m}}$ ) late-type stars in the inner  $5''$  and the dilution of the absorption feature by the concentration of luminous early-type stars there (Krabbe et al. 1995).

The basic premise of the attempts to measure the global properties of the stellar distribution in the inner GC is that there is an underlying dynamically relaxed distribution, which includes most of the mass and most of the stars, and which is traced by the old faint stars. In contrast, the young stars and bright giants, which dominate the light, are less reliable tracers because they could be unrelaxed, or subject to statistical fluctuations due to their small numbers, or susceptible to environmental effects such as stellar collisions or photoionization (Sellgren et al. 1990).

Our current understanding of the stellar distribution in the GC is incomplete. The light distribution approximately follows a  $r^{-2}$  power-law from as far away as  $\sim 100$  pc, where it cannot be directly related to the central super-massive BH, to  $\sim 1$  pc from Sgr A\* (Serabyn & Morris 1996). Previous attempts to characterize the distribution in the inner parsec concentrated on identifying the *core radius*,  $r_c$ , where the surface density falls to half its central value. The value of  $r_c$  is much debated in the literature, and ranges from 0.05 pc (Allen 1983) to  $\sim 1$  pc (Rieke & Rieke 1988). It appears that the differences between the various estimates depend on whether the light distribution or the number counts are used and whether or not the bright stars are included

in the fits.

The most recent estimates for the mass distribution in the inner GC are dynamical and are based on the stellar apparent motions and radial motions. Genzel et al. (1997) and Ghez et al. (1998) fit the enclosed mass estimates to a flattened isothermal distribution of the form

$$\rho(r) = \frac{\rho_0}{1 + 3(r/r_c)^2}, \quad (1)$$

where  $r$  is the 3-dimensional distance from the BH,  $\rho_0 = 4 \times 10^6 M_\odot \text{pc}^{-3}$  and  $r_c = 0.4 \text{ pc}$ . Because the BH mass completely dominates the velocity field at  $r \ll r_c$ , and the stellar mass begins to affect the stellar velocities only at  $r \sim r_c$ , this mass distribution measures only the *integrated* stellar mass up to  $r \sim r_c$ , and is insensitive to the distribution of the stars within the core volume. Therefore, the good fit of the velocity field to this mass model does not necessarily preclude the existence of a stellar cusp in the core.

## 2.2. The $K$ luminosity function and mass function

The construction of the  $K$  luminosity function (KLF) and mass function models for the GC is discussed in detail by Alexander & Sternberg (1999). Briefly, the observed KLF in the GC (Blum et al. 1996; Davidge et al. 1997) can be smoothly joined to that in the Galactic Bulge, as observed through Baade’s window (Tiede et al. 1995), and further extended to lower luminosities by transforming deep optical counts in the bulge (Holtzman et al. 1998) to the  $K$ -band. The resulting KLF (fraction of stars per  $K$ -magnitude) has the form  $df/dK \propto 10^{bK}$  with  $b = 0.35$ , and extends from brightest observed stars in the GC at  $K_1 = 8^{\text{m}}$  down to the main-sequence turnoff at  $K_2 \sim 21.5^{\text{m}}$ . Stars below the main-sequence turnoff at  $\sim 1 M_\odot$  have negligible contribution to the KLF. By normalizing the KLF to the observed star counts in the GC, it can be verified that it reproduces the observed mass-to-light ratio in the GC. This empirical KLF and mass-to-light ratio can also be reproduced remarkably well by a population synthesis model that assumes a continuous star-formation history with a Miller-Scalo (Miller & Scalo 1979; Scalo 1986) initial mass function (IMF) with a mass range of  $0.1 M_\odot$  to  $120 M_\odot$ . The IMF can be then used to follow the evolution of the stellar mass function over time (§5).

We adopt these luminosity and mass functions as a volume averaged description of the stellar population in the inner parsecs of the GC and assume that they adequately describe the “well-mixed” population.

## 2.3. The observed star counts

### 2.3.1. The Keck data set

Ghez et al. (1998) obtained diffraction limited ( $0.05''$  resolution)  $K$ -band images of the inner  $5'' \times 5''$  with the Keck interferometer, down to a detection threshold of  $K_0 = 17^m$ . Using conservative selection criteria, they extracted from the field 90 stars for which the angular motions could be reliably measured and tabulated their magnitude and projected positions and velocities (Figure 1). As the field is slightly off-center with respect to Sgr A\*, only the inner projected  $\sim 2.5''$  are covered over the full  $2\pi$  radians. The original criterion for inclusion in the data set was the reliability of measuring angular motion, rather than completeness in magnitude. Consequently, the counts are complete only down to  $\sim 14^m$ – $15^m$ , beyond where the completeness falls off very rapidly (A. Ghez, private comm.) to a level of  $\gtrsim 1\%$  in the range  $\sim 16^m$ – $17^m$ . The incompleteness is not uniform over the field, as it depends on the distribution of the bright stars. In our analysis we consider only the 64 stars in the inner  $2.5''$ , of which 10 are identified as early type stars. We assume here that the remaining 54 spectrally unidentified stars are late type stars.

### 2.3.2. The OSIRIS data set

Blum et al. (1996) imaged the inner  $2'$  of the GC with the Ohio State Infrared Imager and Spectrometer (OSIRIS) in the  $J$ ,  $H$  and  $K$  bands ( $\sim 1''$  resolution) for the purpose of measuring the luminosity function and color-magnitude diagram of the stellar population. They detected a total of  $\sim 2000$  stars and determined by simulations that the entire sample is complete down to  $K \sim 12^m$ . Of this large sample, they tabulated the  $K$  magnitude, projected positions and  $K$  extinction coefficient  $A_K$  for a sub-sample of 147 stars, which span a range of  $K = 6.4^m$ – $12.4^m$ . The stars included in the sub-sample are those brighter than  $K = 10.5^m$ , those for which Blum et al. obtained  $2\mu\text{m}$  spectra, or those with IRS numbers. Thus, this sub-sample is guaranteed to be complete only down to  $K = 10.5^m$ . The distribution of the stars in the field is very sparse beyond projected radius  $p \sim 10''$ – $15''$  (Figure 2). We limit our analysis to the 50 late type stars in the inner  $13''$  in order not to be affected too much by the Poisson fluctuation in the counts or by molecular gas and dust that may extend inward from the circumnuclear ring (Genzel, Hollenbach & Townes 1994).

### 2.3.3. The 3D and SHARP data set

Genzel et al. (1996) used the 3D imaging spectrometer to identify spectrally 223 stars in the central parsec and separate them into early and late-type stars. The stars were assigned to approximate magnitude classes: bright ( $K \leq 10.5^m$ ), intermediate ( $10.5^m < K \leq 12^m$ ) and faint ( $12^m < K$ ). Because the 3D counts are incomplete in the inner  $5''$  due to source confusion, they augmented the counts with high resolution SHARP camera observations of  $K < 13.5^m$  stars in the inner  $10''$  (Eckart & Genzel 1997), but did not include the 11 very faint ( $K > 14^m$ ) Sgr A\* cluster

stars (S1-S11) in the inner  $\sim 0.5''$  (A. Eckart, private comm.). With the faintest stars excluded from the sample, the composite data set is of roughly uniform depth over the central  $\sim 20''$ .

Genzel et al. (1996) binned the composite data set and fitted a flattened  $r^{-1.8}$  power-law distribution (analogous to Eq. 1) to the surface number density and obtained a core radius of  $r_c = 0.29_{-0.09}^{+0.19}$  pc ( $r_c = 7.4''_{-1.6}^{+5.0}$ )<sup>1</sup>. We reconstruct here the inner  $\sim 20''$  of the the unbinned composite data set for from the tabulated 3D and SHARP stellar positions in order to check whether other density models can fit these star counts as well. Our composite data set includes in total 213 stars, of which 198 are late-type 3D stars from Genzel et al. (1996) and 15 are spectrally unidentified SHARP stars from Eckart & Genzel (1997). The surface distribution of the 213 stars is shown in Fig. 3. To avoid edge-of-field effects, we consider in our analysis below only the 107 late-type stars in the inner  $13''$ , which are composed of 92 3D late-type stars and the 15 SHARP stars.

### 3. Statistical analysis of the star counts

#### 3.1. Stellar density distribution models

The main purpose of this work is to quantify the empirical stellar density distribution in the GC, but theoretical expectations guide us in the choice of models for describing the distribution. Generally, the effect of a super-massive BH on the stellar population within the cusp radius will depend on whether the relaxation time due to two-body stellar encounters is longer or shorter than the system’s age. When two-body relaxation is unimportant, the black hole may grow adiabatically, and the resulting stellar distribution will depend on the initial conditions. A spherically symmetric, non-rotating system that is initially isothermal will develop a  $r^{-3/2}$  cusp (Young 1980). Other initial conditions will result in a variety of density distributions, in some cases as steep as  $r^{-5/2}$  (Lee & Goodman 1989; Quinlan, Hernquist & Sigurdsson 1995).

When two-body encounters are effective, the final configuration will not depend on the initial one. Very close to the BH, where inelastic stellar collisions dominate, a  $r^{-1/2}$  cusp of marginally bound stars will form (Murphy, Cohn & Durisen 1991). At larger radii, where collisions are elastic, a single mass population will settle into a  $r^{-7/4}$  cusp (Bahcall & Wolf 1976). In a realistic stellar population with a spectrum of masses, mass segregation will take place, and the massive stars will be more concentrated towards the center than the low-mass stars. Bahcall & Wolf (1977) investigated the two-body relaxation of a two-component stellar population around a massive BH. They found that the two components settle into different power-law distribution with power-law

---

<sup>1</sup> This is a somewhat smaller value than  $r_c = 10''$  that was adopted in their subsequent works as a compromise between the different core radii suggested in the literature (R. Genzel, private comm.).

indices given by

$$\alpha_i = \frac{m_i}{4m_2} + \frac{3}{2} \quad (m_1 < m_2). \quad (2)$$

Murphy, Cohn & Durisen (1991) showed that Eq. 2 holds also for the spatial distribution of a multi-mass population, when  $m_2$  is taken to be the maximal mass cutoff, so that  $3/2 \leq \alpha_i \leq 7/4$ . It is straightforward to verify that over a limited range in  $r$ , the total density distribution that will be observed will still be an approximate power-law with an index in this range.

The local two-body relaxation time at the core radius of the dynamical mass model (Eq. 1) can be estimated by (Spitzer & Hart 1971)

$$t_r \approx \frac{0.34\sigma^3}{G^2 \langle m \rangle \rho \ln \Lambda} \sim 3 \cdot 10^9 \text{ yr}, \quad (3)$$

where  $\Lambda \approx M_\bullet / \langle m \rangle$  and we assume  $\langle m \rangle = 0.6 M_\odot$ , a BH mass of  $M_\bullet = 2.6 \times 10^6 M_\odot$  (Genzel et al. 1997; Ghez et al. 1998) and  $\rho = 10^6 M_\odot \text{pc}^{-3}$ ,  $\sigma = 117 \text{ km s}^{-1}$  at  $r_c = 0.4 \text{ pc}$  (Genzel et al. 1996). Since the relaxation time is shorter than the age of the Galaxy, the theoretical expectation is that the observed giants, which have an intermediate mass, will have a power-law distribution with an index in the range  $3/2 < \alpha < 7/4$ . However, we will avoid here any theoretical prejudice and investigate power-law distributions with indices that span the full range of the various theoretical scenarios from  $\alpha = 0$  to  $5/2$ .

We consider two spherically symmetric stellar density models. The first is the flattened isothermal model (Eq. 1), where we assume a constant ratio between the mass density and the stellar number density

$$n(r) = \frac{n_0}{1 + 3(r/r_c)^2}, \quad (4)$$

and where  $n_0$  is the central number density and  $r_c = 10''$  (Genzel et al. 1996). The corresponding surface density is

$$\Sigma(p) = \frac{\pi r_c^2 n_0}{3\sqrt{p^2 + r_c^2/3}}, \quad (5)$$

where  $p$  is the projected distance from the center. The second class of models are broken power-laws,

$$n(r) = \begin{cases} n_b (r/r_b)^{-\alpha} & r_0 < r < r_b \\ n_b (r/r_b)^{-\beta} & r \geq r_b, \beta > 1 \end{cases}, \quad (6)$$



where  $n_b$  is the density at the break at  $r_b$ , and  $r_0$  is the closest distance to the BH where stars can exist. Although  $r_b$  is *not* the core radius, we will loosely refer to the region interior to  $r_b$  as the core. The corresponding surface density is

$$\Sigma(p) = n_b \begin{cases} r_b^\beta B\left(\frac{1}{2}, \frac{\beta-1}{2}\right) p^{1-\beta} + 2\sqrt{r_b^2 - p^2} \\ \quad \times \left( H\left(\alpha, \frac{p}{r_b}\right) \left(\frac{p}{r_b}\right)^{-\alpha} - H\left(\beta, \frac{p}{r_b}\right) \left(\frac{p}{r_b}\right)^{-\beta} \right) & r_0 < p < r_b \\ r_b^\beta B\left(\frac{1}{2}, \frac{\beta-1}{2}\right) p^{1-\beta} & p > r_b \end{cases} \quad (7)$$

where  $B$  is the beta function and  $H$  is defined by the hypergeometric function

$$H(x, y) = {}_2F_1\left(\frac{1}{2}, \frac{x}{2}, \frac{3}{2}, 1 - y^{-2}\right). \quad (8)$$

### 3.2. The cumulative distribution function

Figure 4 shows the cumulative distribution functions (DFs) for the late-type stars in the three data sets (more precisely, all the observed stars that were not positively identified as HeI/HI stars, early-type stars or dust embedded stars). The cumulative DFs indicate that neither a flattened isothermal model (Eq. 4) nor a singular isothermal model  $n \propto r^{-2}$  provide a good description of the observed star counts in the central  $\sim 10''$ . This impression is supported by the Kolmogorov-Smirnov (K-S) test results (presented as acceptance probabilities in Table 1), although the K-S scores do not differentiate strongly between the different models. Generally, the K-S scores favor cusps with slopes in the range  $\alpha \sim 3/2$  to  $7/4$ . The discrepancy between the OSIRIS data and the flattened isothermal model is the smallest of all data sets, although this is not the best-fitting model. This probably reflects the fact that the OSIRIS data set is less deep, and is therefore more sensitive to the decrease in the number of luminous late-type giants in the central few arcseconds.

The statistical significance of the concentration of stars at  $p \sim 2''$ , which is seen in the cumulative distribution of the Keck data set, is discussed in appendix A.

### 3.3. Maximum Likelihood analysis

The trends that are seen in the cumulative distributions of the star counts (Figure 4) and the theoretical expectations (§3.1) suggest fitting power-law density distributions to the star counts. In order to avoid the arbitrariness of binning, we perform a Maximum Likelihood (ML) analysis to find the best fitting power-law index  $\alpha$ , assuming a broken power-law distribution

with fixed values  $\beta = 2$  and  $r_b = 10''$  (we verified that the results are not very sensitive to the exact shape of the outer distribution). Figure 5 shows the likelihood curves that were obtained by using Eq. 7 to calculate the relative probabilities of the observed stellar positions<sup>2</sup>. As can be expected, the ML best-fit parameters are not exactly the same as those derived from the Kolmogorov-Smirnov analysis, since the two methods are sensitive to different ranges of the data (the K-S to the mid-range of the projected distance and the ML to the inner, high-probability region). Nevertheless, the results are qualitatively similar. The likelihood curves for all the samples peak in the range  $\alpha \sim 1.5$  to  $1.75$ , irrespective of whether they are based on stars in the inner  $13''$ , or only the inner  $2.5''$ . It is reassuring that this range is consistent with the ML estimate for the entire Keck data set, as this suggests that the contamination by the  $\sim 20\%$  of the young stars does not introduce a large bias. A flat core ( $\alpha = 0$ ) is ruled out only at the  $2\sigma$  level by the Keck and OSIRIS data sets, but is completely incompatible with the 3D+SHARP data.

We also performed a ML analysis to find the best fitting core radius  $r_c$ , assuming a flattened isothermal distribution. The results are qualitatively similar to those of the broken power-law. In all data sets the likelihood curves peak at  $r_c < 2.5''$ , and while a  $10''$  core radius is still compatible with the Keck and OSIRIS data sets at the  $\sim 1.5\sigma$  level, it is ruled out by the 3D+SHARP data at the  $\sim 2.5\sigma$  level.

The best fit core radius we derive from our composite 3D+SHARP data set for the late-type stars ( $r_c = 1.5''$ ) is much smaller than the one derived by Genzel et al. (1996) ( $r_c = 7.4''_{-1.6}^{+5.0}$ ). The reasons for this disparity are unclear. The most significant difference between the two analysis methods appears to be the issue of binning. The binned star counts that were used in the  $\chi^2$  fit of Genzel et al. (1996) could lead to the suppression of a steep cusp in sparse counts. Our initial attempts to fit density models to binned 3D+SHARP data indicated that the best-fit density in the innermost regions fluctuates considerably with small changes in the bin sizes or bin centers. A more detailed comparison of the unbinned ML and the binned  $\chi^2$  fitting procedures, which is outside the scope of this work, will be needed to resolve this issue.

#### 4. Extinction in the inner GC

A gradient in the extinction field could bias the star-counts because fewer stars would be observed where the extinction is higher. For example, a central concentration of dust could make a stellar cusp appear as a flat core, and conversely, a dust ring could make a flat core appear as a cusp. In this section we use observations of the extinction in the GC to estimate the magnitude of such a bias.

---

<sup>2</sup> For each density model, we normalize the probability to the projected distance interval between the innermost and outermost observed stars in the sample. This is necessary for removing biases due to the finite size of the field, and biases due to divergent behavior of the density at  $p = 0$ , where the measured positions are not much larger than the angular resolution and the  $\sim 0.1''$  uncertainty in the position of the dynamic center (Ghez et al 1998).

Davidge (1998) used  $J$ ,  $H$ , and  $K$  observations of stars in the inner  $3'$  to estimate the radial dependence of the  $K$ -band extinction coefficient,  $A_K$ , averaged over  $20''$ -wide bins. Davidge found that  $\langle A_K \rangle$  systematically increases from  $2.8^m$  at  $\sim 100''$  to  $3.2^m$  at  $\sim 30''$ , and then decreases again at the inner  $20''$  to  $2.9^m$  ( $\Delta A_K \sim -0.02^m$  per arcsec). Blum et al. (1996) made a similar study of the inner  $2'$ , and obtained an average central extinction value of  $\langle A_K \rangle \sim 3.3^m$ . Eckart et al. (1995) found no significant color gradient over the Sgr A<sup>\*</sup> cluster in the inner  $1''$ . Figure 6 shows the distribution of stars in the  $A_K - p$  plane in the inner  $25''$  of the GC (Blum et al. 1996). A small fraction of the stars, all concentrated in the inner  $10''$ , are heavily reddened. One of those (IRS 21) was identified by Ott, Eckart & Genzel (1998) as an extended and highly polarized object, which may be a recently formed star still embedded in a dust shell. A second such star (IRS 1W) was also identified in the inner  $10''$ , but is not part of the OSIRIS data set.

The observed total surface density,  $\Sigma_0$ , and the observed differential surface density,  $d\Sigma_0/dA_K$ , reflect the 3-dimensional distribution of the dust. The  $K$ -extinction suffered by a star at projected distance  $p$  and at point  $z$  along the line-of-sight can be decomposed into two parts. The first term,  $A_1(p)$ , corresponds to extinction by a foreground dust screen, and the second term,  $A_2(p, z)$ , corresponds to that by dust inside the GC (Figure 7). The total extinction,  $A_K$ , is then

$$A_K(p, z) = A_1(p) + A_2(p, z) = A_1(p) + D \int_z^\infty d(p, z') dz', \quad (9)$$

where  $d$  is the dust density and  $D$  is a factor that translates the dust column to extinction. Assuming that the unreddened  $K$  luminosity function (KLF) is constant over the volume of interest and assuming cylindrical symmetry around the line of sight, the distribution of stars in the  $p - A_K$  plane is given by  $2\pi p(d\Sigma_0/dA_K)$ , where

$$\frac{d\Sigma_0}{dA_K}(p; K_0) = \left( \frac{\partial z}{\partial A_K} \right)_p n[p, z(A_K)] \int_{K_1}^{K_0 - A_K} \frac{df}{dK} dK \quad \text{for } A_K > A_1(p), \quad (10)$$

and  $K_0$  is the detection limit. The observed total surface density  $\Sigma_0$  will be different from the true one since

$$\Sigma_0(p; K_0) = \int n(p, z) dz \int_{K_1}^{K_0 - A_K(p, z)} \frac{df}{dK} dK. \quad (11)$$

It is important to emphasize that the measured quantity  $\langle A_K(p) \rangle$ , which is averaged over the *observed* stars, is *not* directly related to the average expressed by Eq. 11, since regions of high extinction will be under-represented in the counts, and since intrinsically very luminous stars, which can be observed even through high extinction, are very rare. Therefore, the relatively small measured value  $\langle A_K \rangle \sim 3.5$  does not necessarily preclude the possibility that the innermost GC is hidden by strong extinction. In order to test this, it is necessary to consider the 3-dimensional

distribution of the dust. Because it is unclear what completeness corrections have to be applied to the data presented in Figure 8, we will restrict ourselves here to qualitative comparisons of some simple dust geometries with the observed distribution of stars in the  $p - A_K$  plane.

We consider first the case where the dust is concentrated in a foreground screen, so that  $A_K(p, z) = A_1(p)$ . If  $A_1$  is a constant, or varies randomly over small enough angular scales,  $\Sigma_0$  will simply be proportional to  $\Sigma$ , at least on average, and the extinction will not bias the observed density distribution. This requires us to interpret the few observed highly reddened stars as *intrinsically* reddened objects that do not trace an extended dust distribution. A linear regression of  $A_K$  on  $p$  (Figure 6) does not show any strong systematic trends in the radial behavior of  $A_K$  in the inner  $20''$  and is thus consistent with a foreground dust screen, where the scatter is due to random fluctuations in the extinction, or measurement scatter, or both. The differential extinction is  $\Delta A_K = +0.01^m$  per arcsec based on the the inner  $10''$ , and  $\Delta A_K = -0.03^m$  per arcsec based on the inner  $20''$ , and in both cases  $\Delta A_K = 0$  is within the  $1\sigma$  errors.

The bias due to a non-zero trend of this order will not be large. If a power-law density distribution is estimated from the counts at points  $p_1$  and  $p_2$ , then the difference between the measured power-law index and the true one is

$$\Delta\alpha = \frac{b(p_2 - p_1)\Delta A_K}{\log_{10}(p_2/p_1)}, \quad (12)$$

which is only  $\Delta\alpha < 0.1$  for  $\Delta A_K = -0.03^m$  per arcsec and  $p_1 = 1''$ ,  $p_2 = 10''$ .

Next, we consider the general case, where in addition to a foreground dust screen the BH and the stars near it are embedded in a dust cloud. In particular, we wish to address the possibility that the highly reddened stars in the central  $10''$  are those few stars that are luminous enough to be observed even from inside the dust cloud. We assume a simple configuration where  $A_1$  is constant and the dust is distributed in a spherical cloud with a density profile

$$d = \frac{1}{1 + 3(r/R)^2}, \quad (13)$$

where  $R$  is the core radius of the dust cloud (Figure 7). Figure 8 shows the relative probability density for observing stars in the  $p - A_K$  plane, as calculated from Eqs. 9 and 10, for a  $n \propto r^{-2}$  stellar distribution and a flattened isothermal distribution with a core radius of  $10''$  (Eq. 4). These two stellar distributions were chosen to represent the two cases of a sharp density cusp and a flat core. We set the detection threshold at  $K_0 = 13^m$ , corresponding to the OSIRIS data threshold, and find by trial and error that the parameter values  $D = 0.15$ ,  $R = 30''$  and  $A_1 = 2.5^m$ , which correspond to a maximal extinction of  $10.7^m$ , produce a large enough spread in  $A_K$  at  $\sim 10''$ . Dust models with lower values of  $R$  and  $D$  fail to reproduce the highly reddened stars because they do not have a high enough dust column, while in models with higher values of  $R$  and  $D$  the extinction is so effective that the central  $10''$  is almost completely obscured. Figure 8 show that the models

differ from the observations in several significant aspects. Both predict a strong concentration of stars near and above  $A_1$ , which increases with  $p$  as the extinction decreases. Such an increase is not observed in the data. Both also predict a nearly constant distribution of high- $A_K$  stars from  $p \sim 5''$  outwards (due to the fact that both the dust and stellar columns fall together), unlike the observed distribution, which is confined to the inner  $10''$ . The flat core model predicts very few high- $A_K$  stars in the inner  $\sim 5''$ , since the flat stellar distribution does not provide enough high luminosity stars that can be observed through the dust cloud. This is to be contrasted with the dusty stellar cusp model, which does predict a sparsely populated region in the  $p - A_K$  plane at  $p \lesssim 10''$  and  $A_K \lesssim 7^m$ , approximately as is observed. However, the stellar cusp model also predicts that a strong concentration of highly reddened stars at  $p \lesssim 2''$ , contrary to the observations. We conclude that distributions that are dusty enough to account for the highly reddened stars inside  $10''$  are not favored by the observed distribution of stars in the  $p - A_K$  plane.

However, the  $p - A_K$  distribution in itself cannot rule out a combination of a moderately dusty cloud together with a few intrinsically reddened stars, and furthermore, our conclusions depend on the assumed stellar DF and the KLF. The few spectra that were obtained for stars deep in the potential well can provide additional information that is independent of these assumptions. Such stars can be identified by their high velocities. Genzel et al. (1996) obtained spectra of 4 stars in the Sgr A\* cluster (S1 at  $p = 0.11''$  with projected velocity  $v_\perp = 1556 \text{ km s}^{-1}$ , S2 at  $p = 0.17''$  with  $v_\perp = 691 \text{ km s}^{-1}$ , S8 at  $p = 0.32''$  with  $v_\perp = 1086 \text{ km s}^{-1}$ , and S11 at  $p = 0.54''$  with  $v_\perp = 960 \text{ km s}^{-1}$ ). Assuming that the stars are bound to the  $M_\bullet = 2.6 \times 10^6 M_\odot$  BH (Genzel et al. 1997; Ghez et al. 1998), these velocities translate into maximal 3-dimensional distances from the center of  $r_{\text{max}} = 2GM_\bullet/v_\perp^2 = 0.24'', 1.2'', 0.48'',$  and  $0.62''$ , respectively. The four spectra are featureless and appear to be consistent with those of moderately reddened ( $A_K \sim 3^m$ ) early-type stars in the central cluster (Genzel et al. 1996). This suggests that there is no significant concentration of dust around the BH.

We conclude that spherical dust distributions that are dusty enough to account for the luminous, highly reddened stars in the inner  $10''$  require a stellar cusp to provide enough of such stars and are therefore inconsistent with the absence of a strong concentration of highly reddened stars in the inner few arcseconds. In addition, the absence of a color gradient in the inner  $1''$  and observations of moderately reddened stars deep in the potential well further argue against a central dust cloud. On the other hand, the observed  $p - A_K$  distribution is consistent with extinction by a uniform foreground dust screen, provided that some intrinsically reddened stars exist in the inner  $10''$ . Two such stars have in fact been detected there. A foreground dust screen will not introduce a large systematic bias in the determination of the effective power-law index of the stellar distribution.

## 5. Stellar collisions and the depletion of luminous stars

The problem of the incompleteness of the counts could be circumvented, in principle, by restricting the analysis to the brightest late-type stars, which should directly reflect the projected stellar density. However, stars brighter than  $K = 13.5^m$  are not observed in the inner  $1''$  of the GC in the Keck data set, although the counts are complete at least down to  $K = 14^m$ . Figure 9 shows the distribution of stellar magnitude against projected radius. Apart from the counter-rotating HeI/HI stars, which clearly stand out in the  $p - K$  plane, there is a gradual trend towards a fainter maximal luminosity in the inner  $2''$ . The possibility that this is due to a gradient in the extinction is not supported by the analysis in §4.

Another interesting possibility is that the luminous stars have been destroyed by stellar collisions. Stellar collisions were proposed as the mechanism for destroying the outer envelopes of late-type giants<sup>3</sup> (Lacy, Townes & Hollenbach 1982; Phinney 1989) as an explanation for the depletion of the CO absorption in the integrated light (Sellgren 1990) or for the depletion of the bright late-giants in the counts in the inner  $5''$  of the GC (Genzel et al. 1996). However, the dynamical timescale in the envelope of a giant star is of the order of a year and the thermal timescale is of the order of several decades, so that a collision in which a star “punches a hole” in the giant’s envelope will probably not have a lasting effect. Studies of collisions between dwarf stars and giants indicate that a significant fraction of the collisions can result in a permanent destruction of the envelope if the ratio between the impact parameter and the giant star radius,  $x_e$ , is small enough,  $x_e \lesssim 0.5$ . The envelope is destroyed either by the ejection of the giant’s core from the extended envelope, which then rapidly disperses, or by the formation of a common envelope binary, which stirs the envelope and leads to its evaporation on a time scale much shorter than the giant phase (Livne & Tuchman 1988; Davies & Benz 1991; Rasio & Shapiro 1990, 1991). These studies concentrated on low mass  $\sim 1M_\odot$  giants and on low velocities that are typical of globular clusters, so it is not quite clear how the results scale to higher giant masses and velocities which are typical of the GC. More recently, Davies et al. (1998) proposed that 3-body collisions between binaries and giants may provide a more efficient way of destroying the envelope. They specifically tailored their dynamical simulations to the velocity field and late-type giant masses and envelope sizes that are typical of the GC, and found that envelope-destroying binary–giant collisions require  $x_e$  of order unity. They also concluded that the role of such collisions is negligible in the flat core of the flattened isothermal density model, even if all the dwarf stars are in binaries. These works did not discuss collisional destruction of early-type giant envelopes. However, these are likely to be less effective since it appears that a necessary requirement is that the target star should be composed of two distinct components, a compact core and an extended envelope with a shallow density profile.

---

<sup>3</sup> The  $K$  luminosity of a star of radius  $R$  increases with the effective temperature roughly as  $T_{\text{eff}}$ , so that the  $K$  luminosity scales as  $R^2 T_{\text{eff}}$ , while the bolometric luminosity scales as  $R^2 T_{\text{eff}}^4$ . A giant with  $R = 100 R_\odot$  and  $T_{\text{eff}} = 3 \cdot 10^3$  K that is reduced by a collision to  $\sim 1 R_\odot$  will maintain its bolometric luminosity by raising its effective temperature to  $T_{\text{eff}} = 3 \cdot 10^4$  K, but its  $K$  luminosity will fall by a factor of  $10^3$  ( $7.5^m$ ).

In the following analysis we will assume that 2-body collisions result in the permanent removal of the envelope of a late-type giant if  $x_e \leq 0.25$ . We estimate the efficiency of 3-body collisions by assuming that half of the stars are in binaries. If envelope-destroying binary-giant collisions typically require  $x_e = 1$ , then the effective impact parameter *per dwarf star* is  $x_e = 0.5$  (1 binary per 4 stars, with the collisional cross-section scaling as  $x_e^2$ ). The effective impact parameter per dwarf star must lie somewhere between the 2-body and 3-body values. Therefore, by modeling both types of collisions as 2-body collisions, we are making a conservative estimate of their effectiveness.

Consider first a star on a circular orbit of radius  $r$  around the BH that has total lifetime  $T$  and becomes a giant with a compact core / extended envelope structure after a time  $t_g$ . The Poisson probability for a giant to survive envelope-destroying collisions with dwarf stars up to time  $t > t_g$  is

$$S(t) = \exp\left(-\int_{t_g}^t q(\tau)d\tau\right), \quad (14)$$

where  $q$  is the local collision rate. The collision rate is the sum of a geometrical cross-section term and a gravitational focusing term (see e.g. Binney & Tremaine 1987),

$$q = 4\sqrt{\pi}n_p\sigma(x_e R_t + R_p)^2 \left(1 + \frac{G(M_t + M_p)}{2\sigma^2(x_e R_t + R_p)}\right), \quad (15)$$

where  $n_p$  is the number density of the dwarf projectiles,  $\sigma$  is the 1-dimensional velocity dispersion, and  $M_t$ ,  $M_p$ ,  $R_t$  and  $R_p$  are the masses and radii of the giant targets and dwarf star projectiles, respectively. Both terms have non-negligible contributions over the wide range of stellar masses, radii and velocities in the GC (Eq. B8). Equation 15 assumes a Maxwellian DF with an isotropic velocity dispersion. These conditions appear to hold in the inner GC. The observed radial velocity distribution is well fitted by a Gaussian distribution (Genzel et al. 1996) and is thus consistent with theoretical predictions of the velocity distribution very near a BH (Quinlan, Hernquist & Sigurdsson 1995). The measured velocities in the plane of the sky and along the line-of-sight are consistent with an isotropic velocity dispersion (Ghez et al 1998).

The collision rate  $q$  depends on the position  $r$  through  $n_p$  and  $\sigma$ . The observed isotropic velocity dispersion in the inner GC implies that stars observed at  $r$  have a wide range of orbital parameters and spend a large fraction of their orbital period at distances much larger or much smaller than  $r$ . It is therefore necessary to take into account the fact that the collision rates are not constant along the stellar orbits. As we show in appendix B, when the density and velocity dispersion are power-laws in  $r$ , the orbital averaging modifies Eq. 15 only by introducing two constant correction factors for each of the geometrical cross-section term and the gravitational focusing term. These factors depend on the power-law indices and on the ratio  $\xi = v_c^2/\sigma^2$ , where  $v_c^2 = GM_\bullet/r$  is the circular velocity near the BH.

In our analysis we assume that stars that are not bound to the BH are unaffected by collisions, since the transit time through the inner 0.1 pc is only  $\sim 1000$  yr, which is much shorter than the

typical mean time between collisions ( $> 10^6$  yr). Therefore, the orbit-averaged effective collision rate depends very strongly on the value of  $\xi$ . The larger this ratio is, the smaller the fraction of unbound stars, the more tightly bound the stars whose orbits pass through  $r$  and the longer they spend in the high density regions of the inner GC. The ratio  $\xi$  is related to the stellar density by the Jeans equation, which for a steady-state, non-rotating system with an isotropic potential and isotropic velocity dispersion is

$$\xi \equiv \frac{v_c^2}{\sigma^2} = -\frac{d \ln n}{d \ln r} - \frac{d \ln \sigma^2}{d \ln r}. \quad (16)$$

Near the BH  $v_c^2 \sim GM_\bullet/r$ , so the solution of the Jeans equation for  $n \sim r^{-\alpha}$  is  $\sigma^2 \sim 1/r$  and therefore  $\xi \sim 1 + \alpha$ .

Genzel et al. (1996) assumed a flattened power-law density model (§2.3.3), which is flat ( $\alpha \sim 0$ ) near the BH, and used the Jeans equation to estimate  $\xi$  from the observed projected velocity dispersion  $\sigma_p$ . They assumed a deprojected velocity dispersion of the form  $\sigma^2 = \sigma_\infty^2 + \sigma_c^2(r/r_c)^{-\gamma}$  with  $\sigma_\infty$  a fixed constant, and obtained a best fit value of  $\gamma = 1.2$  and consequently a  $\xi = v_c^2/\sigma^2$  ratio that falls from  $\sim 2$  at  $r \sim r_c$  down to 1.2 at  $r = 0$ . However, their velocity dispersion model is inconsistent with a density cusp. For example, the Jeans equation associates a  $n \propto r^{-2}$  cusp with a smaller deprojected velocity dispersion that varies as  $\sigma^2 = GM_\bullet/3r$ . This can be understood qualitatively by noting that in a flat core the stars have a wider distribution along the line-of-sight and are on average farther away from the BH than they are in a cusp. Therefore, in a flat core a large value of  $\sigma_p$  implies that the stars move at a large fraction of the circular velocity, whereas in a cusp this merely reflects the fact that a larger fraction of the stars are deep in the potential well. A reduction of the velocity dispersion significantly changes the orbital structure of the population. The fraction of stars on orbits more bound than circular ( $v^2 < v_c^2$ ), less bound than circular ( $v_c^2 \leq v^2 < 2v_c^2$ ) and unbound ( $2v_c^2 \leq v^2$ ) are respectively 0.20 : 0.23 : 0.57 for  $\xi = 1$ , 0.43 : 0.31 : 0.26 for  $\xi = 2$ , and 0.61 : 0.28 : 0.11 for  $\xi = 3$ . That is, the steeper the cusp, the more the stars are bound to the black hole. This implies that the stellar population in a flat core is significantly more mixed than it would be in a cusp, and that any local spectral variations in the stellar population will tend to be diluted.

The probability that a star observed at a random time  $t$  during its lifetime will be brighter than some magnitude  $K_0$  is given by

$$P_0 = \frac{1}{T} \left( \int_0^{t_g} m_0(t) dt + \int_{t_g}^T m_0(t) S(t) dt \right), \quad (17)$$

where  $m_0(t)$  is a function that equals 1 when the star is brighter than  $K_0$ , and equals 0 otherwise. The probability  $P_0$  depends on the star's evolutionary track through the fraction of time the star spends in the giant phase and through the evolution of the stellar radius and the  $K$ -luminosity. The probability  $P_0$  has to be averaged over the stellar population to obtain the total probability



of observing any star brighter than  $K_0$ . As was discussed in §2.2, the stellar population in the GC that contributes to the KLF is well modeled by a continuous star-forming history with an approximately Salpeter initial mass function with a minimal mass of  $M_1 = 0.8M_\odot$  and a maximal mass of  $M_2 = 120M_\odot$ , so that the present-day mass function (PMF) can be approximated as

$$\frac{df}{dM_0}(t_0) \propto \Psi \begin{cases} M_0^{-2.35} T & T < t_0 \\ M_0^{-2.35} t_0 & T \geq t_0 \end{cases}, \quad (18)$$

where  $\Psi$  is the star-formation rate, which we take to be constant,  $M_0$  is the zero-age main sequence stellar mass, and  $t_0$  is the age of the system, which we take to be 10 Gyr.

We calculate the PMF-averaged  $P_0$  using the Geneva stellar evolution tracks (Schaerer et al. 1993) for twice-solar metallicity stars and assume blackbody stellar spectra for tracking the  $K$  luminosity with time. We model the stellar DF by a two power-law function (Eq. 6) with  $r_b = 10''$  and  $\rho_b = (3 - \alpha) \times 10^6 M_\odot \text{pc}^{-3}$ , where the pre-factor normalizes all models to have an equal mass of  $\sim 8 \times 10^5 M_\odot$  within  $r_b$ . For the dwarf projectiles (burning stars and stellar remnants), we assume  $n_p(r_b) = \rho_b / \langle m \rangle$  with  $\langle m \rangle = 0.6M_\odot$ , while for the target stars (burning stars only), we assume  $n_t(r_b) = \rho_b / 4$  (see Alexander & Sternberg 1999). The number of stars per  $p$ -annulus that are brighter than  $K_0$  is then given by

$$N(p; K_0) = 2\pi p \Delta p \int_{-\infty}^{+\infty} \int_{M_1}^{M_2} n_t(p, z) [P_0(1 - f_{ub}) + f_{ub}] \frac{df}{dM_0} dM_0 dz, \quad (19)$$

where  $f_{ub}$  is the fraction of unbound stars in the population and where  $P_0$  is calculated with the effective orbit-averaged collision rate as described in appendix B.

We begin by considering a  $r^{-2}$  cusp ( $\xi = 3$  and  $f_{ub} = 0.11$ ). Figure 9 overlays the distribution of the observed stars on a binned gray-scale plot of  $N(p; K_0)$ . The middle contour line shows the model prediction for the values of the minimal magnitude above which less than one star per  $p$ -bin is expected to be observed, with and without collisions. The  $n \propto r^{-2}$  cusp model with collisions reproduces the observed trend to a remarkable degree, given that no attempt was made to fit the data. Apart for the HeI/HI stars, which clearly constitute a separate sub-population, and the other young stars (early-type and dust-embedded stars), there are in total 24 stars below the ‘1 star per  $p$ -bin’ contour. This is statistically consistent with the expected value of 18 for the 18  $p$ -bins between  $0''$  and  $4.5''$ , especially given the possibility that a few of the 24 stars could be unidentified early type stars. The minimal magnitude contour for the no-collisions case clearly fails to reproduce the observations, as it remains flat down to the smallest projected radii. Our model for the collisional depletion of giants predicts that the collisions become effective only at  $p \lesssim 2''$ , which corresponds to  $n_p > 4 \times 10^7 \text{pc}^{-3}$  and  $\sigma > 300 \text{km s}^{-1}$ .

Up to this point we considered only the collisionless orbits of the stars. However, two-body encounters will also affect the orbits. The typical mean time between envelope-destroying collisions in the inner  $2''$  is  $\sim 10^7$  yr per giant, whereas the crossing time of the collisionally-depleted region

is only  $\sim 500$  yr. This raises the question whether the central region can avoid being replenished by collisionally-deflected giants from the dense stellar environment just outside it. A detailed calculation of the replenishment rate is beyond the scope of this work, but we note that there are several reasons that suggest that this process is likely to be inefficient. Slow diffusion of giants into the inner region may make them as vulnerable to collisional destruction as the giants that were originally bound to that region. Giants that will be deflected by a single close elastic collision into a low angular momentum orbit will spend only a small fraction of their lifetime in the central  $2''$ . Moreover, the velocity dispersion in the cusp is high, so that large deflection angles require very close encounters. This defines a collisional radius,  $r_{\text{coll}}$  (Frank & Rees 1976), inside which large deflections require physical (inelastic) collisions. For a  $R_t = 100 R_\odot$ ,  $M_t = 3 M_\odot$  giant, the collisional radius is

$$r_{\text{coll}} = \frac{M_\bullet}{M_t} R_t \sim 2 \text{ pc} \sim 50'' . \quad (20)$$

Therefore, a close encounter within  $x_e r_{\text{coll}}$ , which is close enough to deflect the giant into a low angular momentum orbit, will also destroy its envelope. Replenishment by giants from beyond  $x_e r_{\text{coll}}$  will be less effective because of the lower stellar density there and because of the small angular size of the central  $2''$ , as seen from  $r > x_e r_{\text{coll}}$ .

Next, we consider the case of a flat core ( $\alpha = 0$ ,  $\beta = 2$ ,  $r_b = 10''$  with  $\xi = 1$  and  $f_{ub} = 0.57$ ). Surprisingly, the flat core model shows that the apparent depletion of the high luminosity stars can also be a *projection* effect. Figure 9 shows that collisions play no role in such a low density models, in agreement with the conclusion of Davies et al. (1998) but contrary to the suggestion of Genzel et al. (1996). However, since the number of stars per  $p$ -annulus falls as  $p$  in a flat core, the probability of observing one of the rare luminous star also falls with  $p$ . This is to be contrasted with the  $r^{-2}$  cusp, where the number of stars per annulus is constant.

The origin of the depletion in a  $r^{-2}$  cusp is collisional, while in a flat core it is due to a projection effect<sup>4</sup>. Stellar cusps shallower than  $r^{-2}$  will display both types of depletion. Close inspection of the predicted depletion in the  $r^{-2}$  cusp (Fig. 9) shows that it somewhat underestimates the depletion at the smallest projected distances, and that a better fit can be obtained by a shallower cusp, for example  $r^{-3/2}$ .

We conclude that the depletion of the bright stars in the inner  $2''$  can be explained by a combination of collisional destruction of giant envelopes, which requires the high densities of a stellar cusp, and by projection effects. The latter is due to the fact that density distributions that are shallower than a  $r^{-2}$  cusp have progressively less stars enclosed in smaller projected radii, and so there is a smaller chance of observing the rarer, more luminous stars there. Because of the degeneracy between the collisional depletion and the projection effects, the distribution of the

---

<sup>4</sup> A  $r^{-\alpha}$  cusp with  $\alpha > 2$  will have collisional depletion offset by apparent *enhancement* due to projection.

brightest stars alone cannot decide the case between a flat core and a cusp.

## 6. Discussion

### 6.1. The star counts

The analysis of the star counts is not straightforward and must overcome several difficulties. First, the observed star-counts have yet to be published in a way suitable for detailed analysis by taking into account completeness corrections and field edge corrections. Second, the GC contains a population of luminous young stars, which are not dynamically relaxed, and therefore introduce noise in the counts. Third, a gradient in the extinction field may bias the counts. Although none of these concerns can be completely eliminated, we have attempted to minimize their possible effects in our analysis.

An important aspect of our effort to control the effects of incompleteness was the use of three different data sets, with different properties and biases. We analyzed them in a uniform way by methods that avoid binning, as is appropriate when dealing with sparse data. It is reassuring that all three data sets indicate that a cusp matches the counts better than a flat core. The case for a cusp is further strengthened by the fact that both incompleteness due to source confusion and a central concentration of dust will tend to suppress the observed cusp. Another way of circumventing the completeness problem is to consider the information in the distribution of the brightest stars. We discuss this further below.

We attempted to limit the contamination by the young unrelaxed population by excluding all the identified young stars from the data sets. Although we do not know how many of the fainter stars are associated with this unrelaxed population, the star-burst model of Krabbe et al. (1995) predicts that their fraction should become negligible as the counts go deeper. It is possible that this trend is already apparent in the differences between the OSIRIS data set and the two other deeper data sets (Figure 4). The ML power-law index does not change significantly when the young stars are included in the sample (Figure 5).

To estimate the possible effects of extinction gradients, we constructed a few simple 3-dimensional dust distribution models and tested them against the observed distribution of stellar extinction in the projected distance–reddening plane. We find that on the  $\sim 10''$  scale, the observations are consistent with an external dust screen, which is unlikely to significantly bias the derived power-law index of the stellar distribution. Our constraints on variations on  $\sim 1''$  scales are weaker, but we note that the detection of moderately reddened stars very deep in the potential well is consistent with little reddening in the innermost GC, and that no significant color gradient was detected in the inner  $1''$ .

These precautions and checks are no substitute for better data. Clearly, deep, completeness-corrected data sets are desirable. A comparison of the likelihood curves of the Keck and

3D+SHARP data set shows that even a two-fold increase in the sample size from  $\sim 50$  to  $\sim 100$  can lead to a significant improvement in the ability to discriminate between stellar distribution models. Our KLF model suggests a two-fold increase in the number of stars observed for every  $1^m$  improvement in the photometric sensitivity.

## 6.2. The depletion of bright stars

In addition to the analysis of the total star counts, we examined the distribution of the counts as function of magnitude and noted that the highest resolution data set shows a gradual depletion of the brightest stars in the inner  $2''$  (a reflection of the fact that there are no bright stars in the Sgr A\* cluster). Reproducing this effect by reddening would require a  $\sim 2.5^m/2''$  extinction gradient, which is not indicated by our analysis (§4). We showed that envelope-destroying collisions between dwarfs and giants can reproduce the observed trend to a remarkable degree, once the young unrelaxed stars are excluded from the data set. Our detailed model for the effects of collisions on the luminosity function included six components: realistically lowered estimates for the cross-section of envelope-destroying collisions, based on results from hydrodynamical simulations of dwarf-giant collisions; an orbit-averaged estimate of the collision rate; a velocity dispersion model that is self-consistent with the assumed density distribution; a stellar mass function that reproduces the mean observed  $K$  luminosity function and mass-to-light ratio; stellar tracks that model the evolution of the size and luminosity of the stars as function of their initial mass; and a careful statistical treatment of the survival probability.

Our dynamical analysis shows that a cusp is necessary for collisional depletion to play a role because the process becomes effective only at a density of order  $> 5 \times 10^7 M_\odot \text{pc}^{-3}$  with a velocity dispersion of order  $> 300 \text{ km s}^{-1}$ , and because a cusp is much more tightly bound to the BH than a flat core. The unbound stars spend too little time in the high density central regions to be affected by the collisions, and so set an upper limit on the fraction of giants in the population that can be effectively destroyed.

Stellar collisions are only one way to explain the absence of bright stars without having to invoke intrinsic variations in the stellar population. We also find that a flat core can qualitatively mimic such a depletion by a projection effect, even when collisions play no role. This explanation for the absence of bright stars in a flat core may actually be more likely than to assume intrinsic variations in the stellar population. Any localized, distinct stellar population in a flat core will be diluted by the large fraction of loosely bound stars that sample the population from over the entire GC.

### 6.3. Implications of a stellar cusp in the GC

We now discuss briefly some of the implications of the existence of a steep stellar cusp in the GC. The tidal disruption rate of stars by the BH is enhanced in a steep cusp. Such events may be observed as short and luminous flares (Rees 1988). Bahcall & Wolf (1977) estimated the diffusion rate into the ‘loss-cone’ (low angular-momentum orbits) as function of the BH mass and of the line-of sight velocity dispersion and the stellar density outside the cusp. Adopting a broken power-law density distribution (Eq. 6) with  $r_b = 10''$ ,  $\beta = 2$  and  $n_b = 10^6 \text{ pc}^{-3}$  and taking  $\sigma_p \sim 85 \text{ km s}^{-1}$  at  $\sim 2.5 \text{ pc}$  from Kent (1992) or  $\sigma_p \sim 60 \text{ km s}^{-1}$  at  $\sim 4 \text{ pc}$  from Genzel et al. (1996), we estimate a loss-cone diffusion rate of  $\text{few} \times 10^{-5} \text{ yr}^{-1}$ . This is consistent with the rates derived by Magorrian & Tremaine (1999) for faint galaxies ( $L < 10^{10} L_\odot$ ) with low-mass BHs and steep density cusps, but is much larger than the  $10^{-9} - 10^{-8} \text{ yr}^{-1}$  rates that they derived for  $L^*$  galaxies. Magorrian & Tremaine suggest that tidal flares are most likely to be detected in faint galaxies. Our results raise the possibility that at least some luminous galaxies may have tidal flare rates as high as those of faint galaxies.

Inelastic dwarf–dwarf collisions are expected to modify the stellar distribution in the inner, highest density regions of the cusp by gradually destroying the tightly bound stars. This leads to the formation of a  $n \propto r^{-1/2}$  cusp of unbound stars. The relevant time-scale for this process is the time it takes to destroy a star by successive collisions. Murphy, Cohn and Durisen (1991) show that the collisional destruction timescale is  $\gtrsim 10t_{\text{coll}}$ , where  $t_{\text{coll}}$  is the collision timescale per star. The size of the unbound cusp that they derive in two of their numerical models that roughly bracket the conditions in the GC (models 3B and 4B), is  $0.002 < r_d < 0.04 \text{ pc}$  at 15 Gyr. This qualitatively agrees with our independent estimate of  $t_{\text{coll}} \lesssim 5 \times 10^8 \text{ yr}$  at  $r < 0.02$  for dwarf–dwarf collisions in a  $\alpha = 1.5$  cusp. We therefore expect the cusp to flatten somewhere within  $p \lesssim 0.5''$ . We estimate that dwarf–dwarf inelastic collisions occur in that volume at a rate of  $10^{-5} - 10^{-4} \text{ yr}^{-1}$ .

A steep stellar cusp will also increase the rate of microlensing of stars by the BH (Alexander & Sternberg 1999), and especially that of short duration microlensing events of stars very near the BH. Such microlensing light-curves can be used, in principle, to probe the mass distribution of the central dark mass and test whether it is a point mass. These issues will be discussed in more detail elsewhere.

Finally, we note that the integrated stellar mass close to the black hole is very small in spite of the very high density of the cusp. For example, the stellar mass within  $2''$  in a  $r^{-2}$  cusp is  $\sim 8 \times 10^4 M_\odot$  as compared to only  $\sim 8 \times 10^3 M_\odot$  in the flattened isothermal distribution (when both are normalized to have the same mass within  $r_c = 10''$ ). This difference amounts to only a  $\sim 3\%$  over-estimate in the BH mass due to the fact that some of the stellar mass is erroneously attributed to the BH.

## 7. Summary

Recent deep high-resolution observations of the inner GC and large scale multi-color observations have supplied a wealth of information on the spatial distribution of stars near the super-massive BH in the GC. This offers the opportunity to map the stellar distribution around the BH directly from the star counts, rather than from the integrated light. Dynamical scenarios predict that a stellar cusp should form around the BH, and that the shape of the cusp could provide clues on the formation history of the BH and the stellar system around it. It is therefore puzzling that recent empirical GC mass models indicate a flat core rather than a cusp, while at the same time, deep observations reveal an over-density of faint stars and an absence of bright stars in the inner  $1''$  (the Sgr A\* cluster). Taken at face value, this picture raises several questions: What does the absence of a cusp imply about the dynamical state of the GC? Are the faint stars a distinct population? If so, how have they formed in the inner  $1''$  or how have they migrated there? Our analysis of three independent sets of star counts points to a simpler interpretation of these findings. Our main results are as follows.

1. The central over-density is likely the tip of a stellar cusp that rises smoothly in the inner  $\sim 10''$ . A stellar cusp is consistent with the star-counts and is preferred at the  $\sim 2\sigma$  level over a flat core distribution even by the least restrictive data set. A flat core is completely ruled out by the largest data set. The maximum likelihood range for the power-law index of the cusp is  $\alpha \sim 1.5$  to  $1.75$ . An alternative way of stating this result is that our analysis points to a small core radius,  $r_c < 2.5''$ .
2. The gradual depletion of the luminous giants in the inner  $2''$  can be explained by two effects: envelope-destroying dwarf-giant collisions in a steep, dense and tightly bound cusp, or a projection effect in a flatter distribution, where the number of stars per projected annulus falls with decreasing projected radius. The observed depletion in the innermost regions is better described by a  $\alpha < 2$  cusp, where both effects contribute. Either way, it is unnecessary to assume that the stellar population in the innermost GC is intrinsically different (fainter) from the general population.
3. The *joint constraints* of the star counts and the depletion of the brightest stars suggest that a power-law cusp with  $\alpha$  in the range  $3/2$  to  $7/4$  provides a good overall description of the data. Such a cusp is consistent with the Bahcall-Wolf solution (Bahcall & Wolf 1976, 1977; Murphy, Cohn & Durisen 1991; see §3.1) for the distribution of intermediate mass stars in a multi-mass stellar system that has undergone two-body relaxation around a black hole (Eq. 2). Dynamical estimates (Eq. 3) suggest that the inner GC is relaxed. If future deeper star counts support these conclusions, this would be the first detection of such a system.

I am grateful to A. Eckart, R. Genzel and A. Ghez for supplying additional information about their data and to J. Bahcall, D. Eisenstein, J. Goodman and S. Tremaine for helpful comments.

### A. The stellar “ring” at $2''$

Is the striking over-concentration of stars in a thin ring at  $p \sim 2''$ , which is seen in the cumulative distribution of the Keck data set (Figs. 1 and 4), inconsistent with a power-law distribution (9 late-type stars in a ring of width  $0.06''$  out of a total of 54 late-type star or 11 stars of all spectral types out of a total of 64 stars)? This is probably not an instrumental artifact, since it is seen also in the full OSIRIS data set. The 11 stars do not seem to have any other peculiar characteristics apart from their spatial alignment. Only two (16CC and 29N) are identified as HeI/HI stars (Eckart & Genzel 1997), their mean magnitude of  $\overline{K} = 12.6^{\text{m}} \pm 2.9^{\text{m}}$  is consistent with the total average of  $\overline{K} = 13.4^{\text{m}} \pm 2.8^{\text{m}}$ , and their projected velocity vectors appear to be random. In order to address this question, we performed Monte-Carlo simulations where we randomly drew 64 stars from a  $n \propto r^{-\alpha}$  distribution and recorded the number of times a group of  $k$  stars or more was concentrated within a ring of  $\Delta p = 0.06''$  or less, for various values of  $k$  and  $\alpha$  (a ring of  $k$  stars is counted twice if it is a subset of a ring of  $k + 1$  stars). The distribution of the ring radii was also recorded. The results, listed in table 2, show that a ring of 11 stars in  $0.06''$  is quite rare in a  $\alpha = 2$  model, where there are on average only  $2.3 \cdot 10^{-5}$  such rings per random realization, with radii  $1.3'' \pm 0.7''$ , but less rare in the flatter  $\alpha = 3/2$  model, where the average number is  $2.3 \times 10^{-4}$  with radii  $2.1'' \pm 0.3''$ . The probabilities increase by more than an order of magnitude if only the 9 late-type stars are considered members in the ring.

The Monte-Carlo averaged ring position reflects a trade-off between the ring area, which increases with  $p$ , and the density distribution, which decreases with  $p$ . Therefore, both the probability for observing a ring, and the ring’s radius, increase in flatter distributions. The fact that an 11-star ring of radius  $2''$  is observed, can be turned around and used as a Maximum Likelihood argument in favor of a flatter inner distribution. Future deeper number counts will show whether this feature is more than a statistical fluctuation.

### B. The effective orbit-averaged collision rate

We estimate the corrections to the local collision rate (Eq. 15) due to the fact that the stars are not on circular orbits by making two simplifying assumptions. First, we assume that the stars in the inner GC move on Keplerian orbits around the BH, so that the orbits can be parameterized by their semi-major axis  $a$  and their eccentricity  $e$ . Second, we assume that unbound stars are unaffected by collisions (see §5). When the orbital period  $P$  of a star around the BH is shorter than the giant phase, the orbit-averaged collision rate is

$$\bar{q}(r, a, e) = \frac{2}{P} \int_{a(1-e)}^{a(1+e)} q(s) \frac{ds}{s}, \quad (\text{B1})$$

where  $s$  is the radial coordinate of the orbit and  $a(1 \pm e)$  are the apoastron and periastron radii, respectively. The radial velocity varies with  $s$  as

$$\dot{s}^2 = 2 \left( \epsilon + \frac{GM}{s} \right) - \frac{h^2}{s^2}, \quad (\text{B2})$$

where  $\epsilon = -GM_{\bullet}/2a$  is the specific energy and  $h = \sqrt{GM_{\bullet}a(1-e^2)}$  is the specific angular momentum of the star. The orbital parameters of a star at  $r$  with velocity  $v$  can be expressed in terms of  $\tilde{v} = v/\sigma$  and the angle between the radius and the velocity vectors,  $\eta$ ,

$$a = \frac{r}{2 - \tilde{v}^2/\xi}, \quad (\text{B3})$$

$$e^2 = 1 + \sin^2 \eta \left( \frac{\tilde{v}^4}{\xi^2} - \frac{2\tilde{v}^2}{\xi} \right), \quad (\text{B4})$$

where  $\xi = v_c^2/\sigma^2$ . For  $n \propto r^{-\alpha}$  and  $\sigma^2 \propto r^{-\gamma}$ , the geometrical cross-section term and the gravitational focusing term in the local collision rate can be expressed as  $q(r) = q_g + q_f = Ar^{-(\alpha+\gamma/2)} + Br^{-(\alpha-\gamma/2)}$ , where the constants  $A$  and  $B$  are defined by Eq. 15. In this case, the corresponding orbit-averaged terms are

$$\bar{q}_{g,f}(r) = \left[ (2 - \tilde{v}^2/\xi)^{(\alpha \pm \gamma/2)} \frac{\sqrt{x_1 x_2}}{\pi} \int_{x_1}^{x_2} \frac{x^{\alpha \pm \gamma/2 - 2} dx}{\sqrt{(x-x_1)(x_2-x)}} \right] q_{g,f}(r) \equiv C_{g,f}(\tilde{v}, \eta) q_{g,f}(r), \quad (\text{B5})$$

where  $x_{1,2} = 1/(1 \pm e)$  and where the (+) case corresponds to  $\bar{q}_g$  and the (-) case to  $\bar{q}_f$ . It then follows that  $\langle \bar{q} \rangle_{g,f}$ , the averages of  $\bar{q}_{g,f}$  over the Maxwellian DF of the bound stars, are related to the local collision rates  $q_{g,f}$  by proportionality factors that are functions of the constants  $\alpha$ ,  $\gamma$  and  $\xi$  but not of  $r$ ,

$$\langle C \rangle_{g,f} \equiv \langle \bar{q} \rangle_{g,f} / q_{g,f} = (2\pi)^{-1/2} \int_0^{\sqrt{2\xi}} \int_0^\pi C_{g,f}(\tilde{v}, \eta) \tilde{v}^2 \exp(-\tilde{v}^2/2) \sin \eta d\tilde{v} d\eta. \quad (\text{B6})$$

In practice, the expectation value  $\langle C \rangle$  diverges for certain choices of  $\alpha$  and  $\gamma$  due to low angular-momentum orbits that sample regions of diverging density and velocity dispersion. For this reason, and because the survival probability (Eq. 14) is a highly non-linear function of the collision rate, a more relevant quantity is the *median* correction factor  $\widehat{C}$ , defined as the ratio between the median of  $\bar{q}$  over the population of bound stars and the local rate  $q$ . Table 3 lists  $\widehat{C}_f$  and  $\widehat{C}_g$  for different density distributions that may be relevant in the inner GC, as well as the fraction of unbound stars,  $f_{ub}$ , that corresponds to each value of  $\xi$ . The median correction factors were estimated by  $10^6$  Monte Carlo draws of random velocity vectors from the DF. Using these factors, the effective collision rate for the bound stars is estimated by

$$q_{\text{eff}} = A\widehat{C}_g r^{-(\alpha+\gamma/2)} + B\widehat{C}_f r^{-(\alpha-\gamma/2)}. \quad (\text{B7})$$



The relative contributions of the geometrical cross-section term and the gravitational focusing term to the effective collision rate is (cf. Eq. 15)

$$\left(\frac{q_g}{q_f}\right)_{\text{eff}} = \frac{\widehat{C}_g}{\widehat{C}_f} \frac{2}{\xi} \left(\frac{M_\bullet}{M_t + M_p}\right) \left(\frac{x_e R_t + R_p}{r}\right). \quad (\text{B8})$$

This ratio can be both much larger than 1 or smaller than 1 over the wide range of stellar masses, radii and distances in the GC, so that both terms should be taken into account when calculating  $q_{\text{eff}}$ .

## REFERENCES

- Alexander, T., & Sternberg, A., 1999, *ApJ*, 520, in press
- Allen, D. A., Hyland, A. R., & Jones, T. J., 1983, *MNRAS*, 204, 1145
- Bahcall, J. N., & Wolf, R. A., 1976, *ApJ*, 209, 214
- Bahcall, J. N., & Wolf, R. A., 1977, *ApJ*, 216, 883
- Binney, J., & Tremaine, S., 1987, *Galactic Dynamics*, (Princeton University Press: Princeton), p. 541
- Blum, R. D., Sellgren, K., & DePoy, D. L., 1996, *ApJ*, 470, 864
- Carney, B., Fulbright, J. P., Terndrup, D. M., Suntzeff, N., & Walker, A., 1995, *AJ*, 110, 1674
- Davidge, T. J., 1998, *AJ*, 115, 2374
- Davidge, T. J., Simons, D. A., Rigaut, F., Doyon, R., & Crampton, D., 1997, *AJ*, 114, 2586
- Davies, M. B., & Benz, W., 1991, *ApJ*, 381, 449
- Davies, M. B., Blackwell, R., Bailey, V. C., & Sigurdsson, S., 1998, *MNRAS*, 301, 745
- Eckart, A., & Genzel, R., 1997, *MNRAS*, 284, 576
- Eckart, A., Genzel, R., Hofmann, R., Sams, B. J. & Tacconi-Garman, L. E., 1993, *ApJ*, 407, L77
- Eckart, A., Genzel, R., Hofmann, R., Sams, B. J. & Tacconi-Garman, L. E., 1995, *ApJ*, 445, L23
- Frank, J., & Rees, M. J., 1976, *MNRAS*, 176, 633
- Ghez, A. M., Klein, B. L., Morris, M., & Becklin, E. E. 1998, *ApJ*, 509, 678
- Genzel, R., Hollenbach, D., & Townes, C. H., 1994, *Rep. Prog. Phys.*, 57, 417
- Genzel, R., Eckart, A., Ott, T. & Eisenhauer, F. 1997, *MNRAS*, 291, 21
- Genzel, R., Thatte, N., Krabbe, A., Kroker H. & Tacconi-Garman, L. E. 1996, *ApJ*, 472, 153
- Holtzman, J. A., et al., 1998, *AJ*, 115, 1946
- Lacy, J. H., Townes, C H., & Hollenbach, D. J., 1982, *ApJ*, 262, 120
- Lee, M.-H., & Goodman, J., 1989, *ApJ*, 343, 594
- Livne, E., & Tuchman, Y., 1988, *ApJ*, 332, 271
- Kent, S. M., 1992, *ApJ*, 387, 181

- Kormendy, J., & Richstone, D., 1995, *AR&A*, 33, 581
- Krabbe, A., et al., 1995, *ApJ*, 447, L95
- Magorrian, J., et al., 1998, *AJ*, 115, 2285
- Magorrian, J. & Tremaine S., 1999, *MNRAS*, submitted (astro-ph/9902032)
- Miller, G. E., & Scalzo, J. M., 1979, *ApJS*, 41, 513
- Morris, M., & Serabyn, E., 1996, *ARA&A*, 34, 645
- Murphy, B. W., Cohn, H. N., & Durisen, R. H., 1991, *ApJ*, 370, 60
- Ott, T., Eckart, A., & Genzel, R., 1998, *ApJ* submitted
- Phinney, E. S., 1989, in *The Center of the Galaxy*, ed. M. Morris (Dordrecht: Kluwer), 543
- Quinlan, G. D., Hernquist, L., & Sigurdsson, S., 1995, *ApJ*, 440, 554
- Rasio, F. A., & Shapiro, S. L., 1990, *ApJ*, 354, 201
- Rasio, F. A., & Shapiro, S. L., 1991, *ApJ*, 377, 559
- Rees, M., 1988, *Nature*, 333, 523
- Rieke, G. H., & Rieke, M. J., 1988, *ApJ*, 330, L33
- Scalo, J. M., 1986, *Fundam. Cosmic. Phys.*, 11, 1
- Schaerer, D., Charbonnel, C., Meynet, G., Maeder, A., & Schaller, G., 1993, *A&AS*, 102, 339
- Sellgren, K., McGinn, M. T., Becklin, E. E., & Hall, D. N. B., 1990, *ApJ*, 359, 112
- Serabyn, E., & Morris, M. 1996, *Nature*, 382, 602
- Serabyn, E., Shupe, D., & Figer, D. F. 1998, *Nature*, 394, 448
- Spitzer, L. & Hart, M. H., 1971, *ApJ*, 164, 399
- Tiede, G. P., Frogel, J. A., & Terndrup, D. M., 1995, *AJ*, 110, 2788
- Young, P., 1980, *ApJ*, 242, 1232

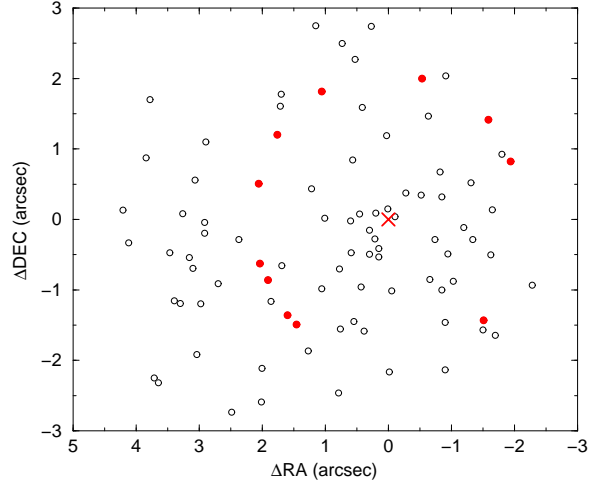


Fig. 1.— 90 stars in the inner  $\sim 6'' \times 6''$  observed by the Keck interferometer (Ghez et al. 1998). Stars marked by filled circles constitute the “ring” feature (Appendix §A). Only the 64 stars in the central  $2.5''$  (of which 10 are early-type stars) are used in the analysis.

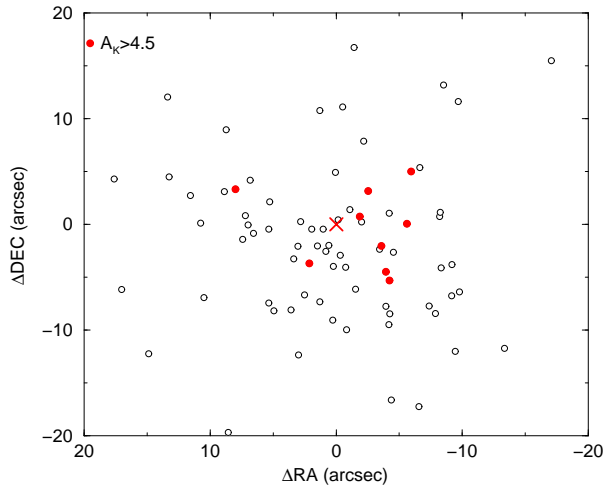


Fig. 2.— The inner  $40'' \times 40''$  of the OSIRIS field (Blum et al. 1996). Stars marked by filled circles are highly reddened stars ( $A_K > 4.5^m$ ). Only the 50 late-type stars in the inner  $13''$  are used in the analysis.

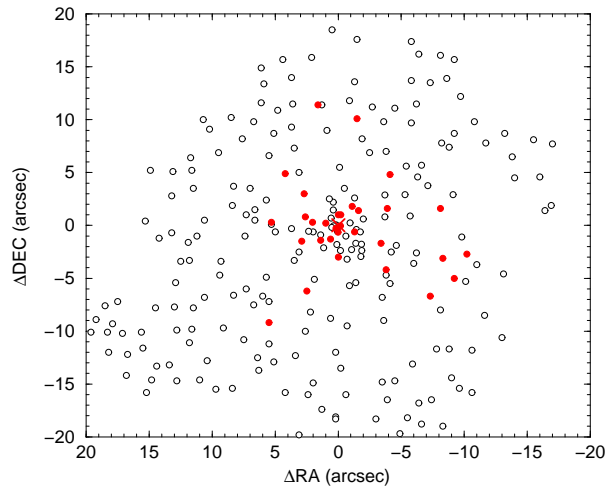


Fig. 3.— The combined 3D (Genzel et al. 1996) and SHARP (Eckart & Genzel 1997) counts in the inner  $20''$ . Stars marked by filled circles are identified HeI/HI and early-type stars. Only the 92 late-type 3D stars and the 15 spectrally unidentified SHARP stars (excluding the faint Sgr A<sup>\*</sup> cluster stars) in the inner  $13''$  are used in the analysis.

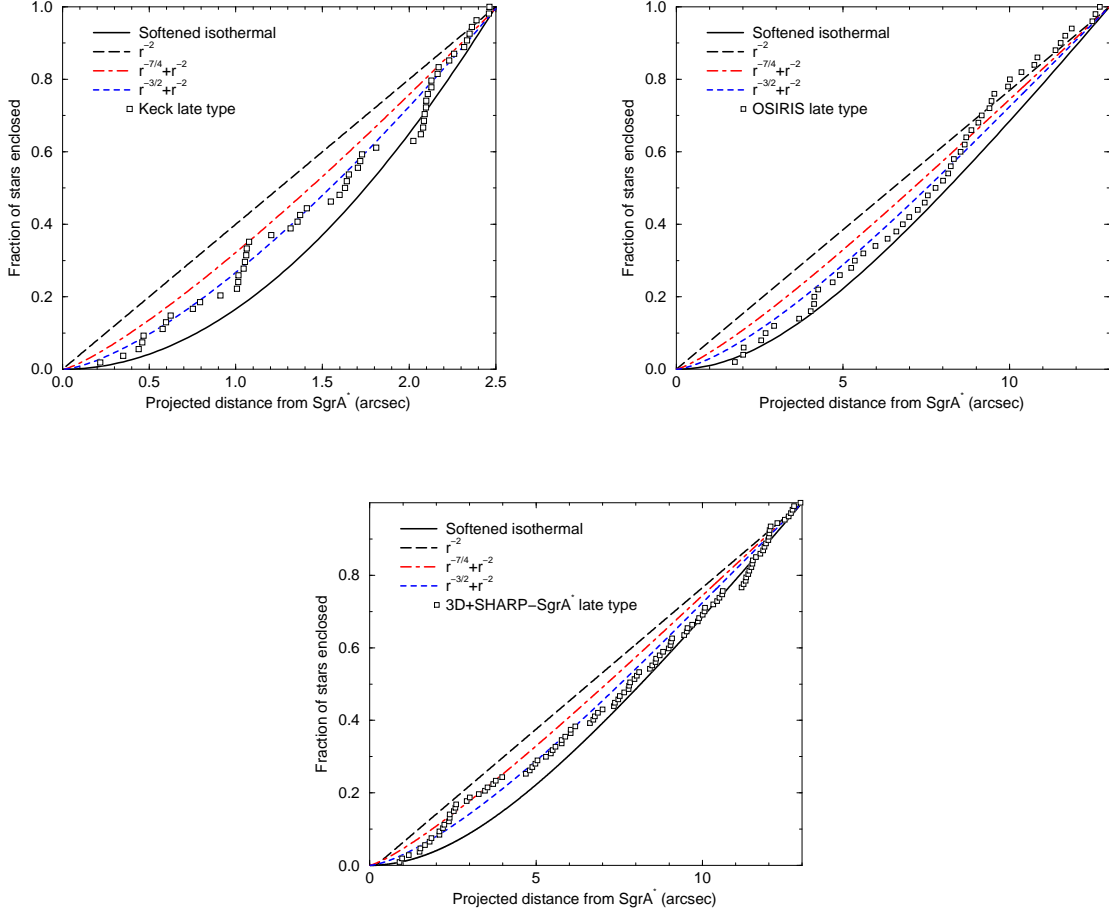


Fig. 4.— The cumulative DF of the late-type stars for the different data sets, compared to various stellar density distribution models. Top left: the inner  $2.5''$  of the Keck field (Ghez et al. 1998). Top right: the inner  $13''$  of the OSIRIS field (Blum et al. 1996). Bottom: the inner  $13''$  of the 3D field (Genzel et al. 1996) together with the inner  $10''$  of the SHARP data excluding the faint Sgr A\* cluster stars (Eckart & Genzel 1997).

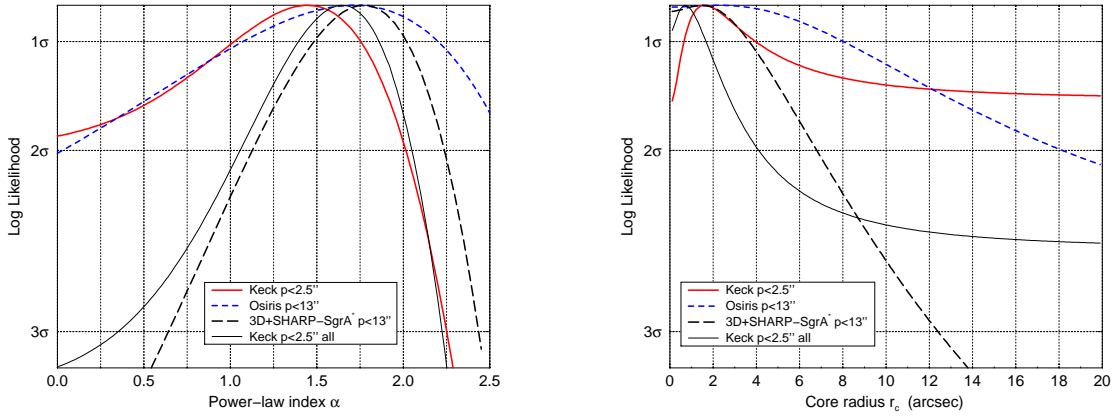


Fig. 5.— The ML estimate of the stellar distribution for the late-type stars in the three data sets. The likelihood curves for the full Keck data set (including early-type stars) is also presented for comparison. Left: The likelihood curves for the power-law index  $\alpha$  of the broken power-law distribution, for fixed values of  $\beta = 2$ ,  $r_b = 10''$ . Right: The likelihood curves for the core radius  $r_c$  of the flattened isothermal distribution.

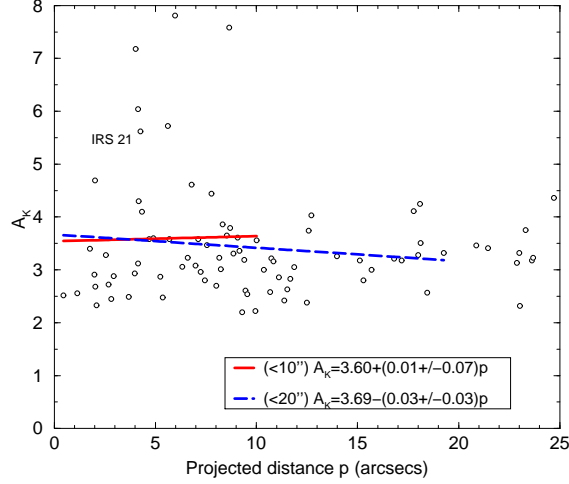


Fig. 6.— The extinction of individual stars in the inner 25'' of the GC deduced from the near infrared colors (Blum et al. 1996). The average error on the extinction estimate is  $\sim 0.1^m$  (not including systematic error due to the assumed intrinsic colors). The linear regression of  $A_K$  on  $p$  in the inner 10'' and 20'' is also shown. IRS 21 is a highly polarized extended object (Ott, Eckart & Genzel 1998).

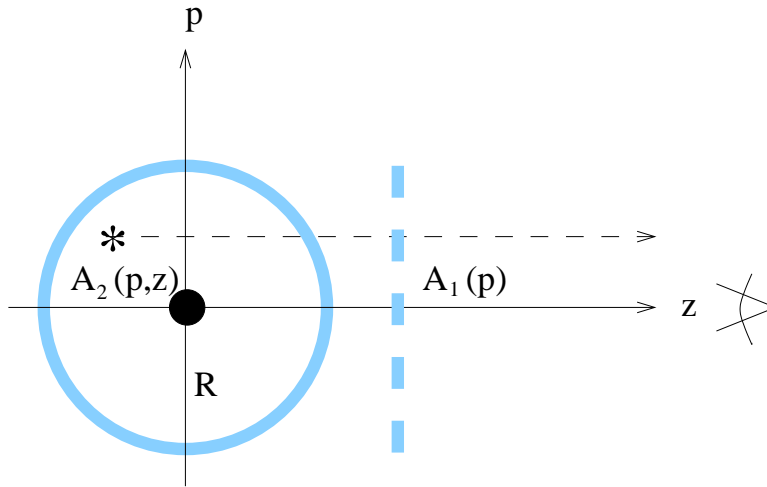


Fig. 7.— A simple trial model for the extinction field in the GC. A star at projected distance  $p$  and point  $z$  along the line-of-sight, is embedded in a spherical dust cloud of core radius  $R$  that surrounds the black hole. The total extinction is the sum of the extinction due to dust inside the cloud,  $A_2(p, z)$ , and to dust in a foreground screen,  $A_1(p)$ .



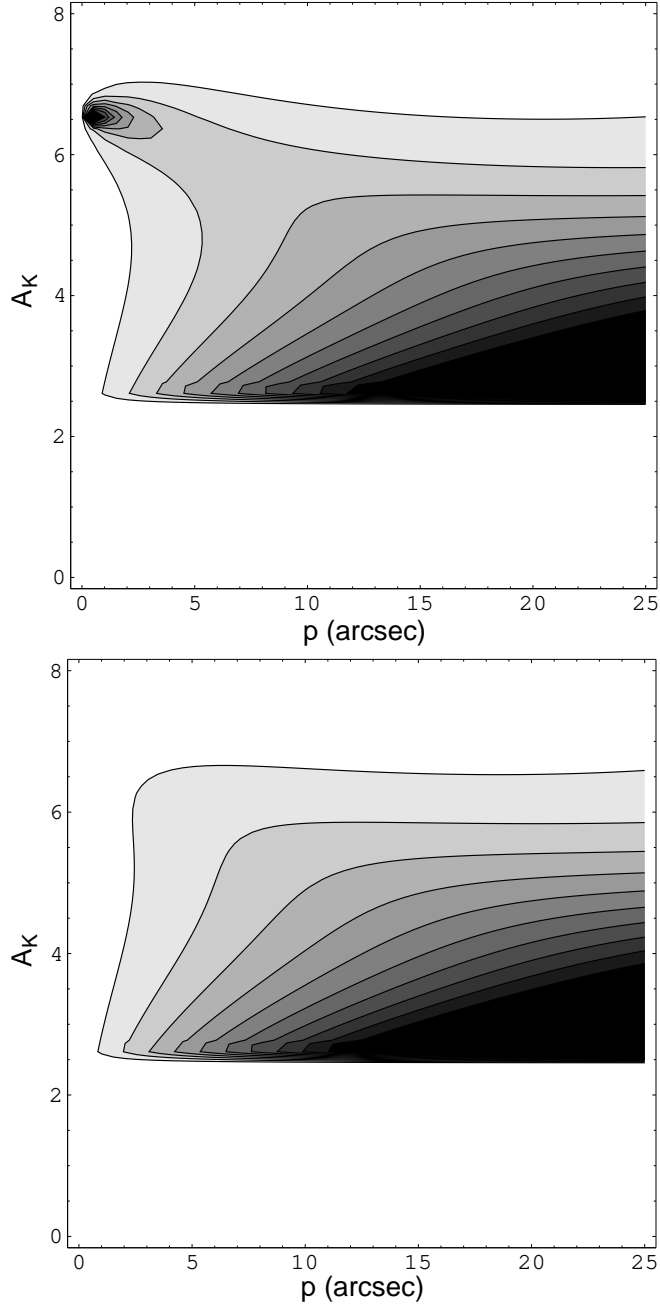


Fig. 8.— The relative probability density (normalized to the peak) for the detection of stars at projected distance  $p$  and extinction  $A_K$ . The dark regions correspond to high detection probability. Top: a  $n \propto r^{-2}$  stellar distribution. Bottom: a flattened isothermal model (Eq. 4). The assumed dust model is a spherical  $d = 1 / (1 + 3(r/R)^2)$  distribution with  $R = 30''$ ,  $D = 0.15$ , and  $A_1 = 2.5^m$ , the luminosity function is  $df/dK \propto 10^{bK}$  with  $b = 0.35$ , and the detection threshold is  $K_0 = 13^m$ .

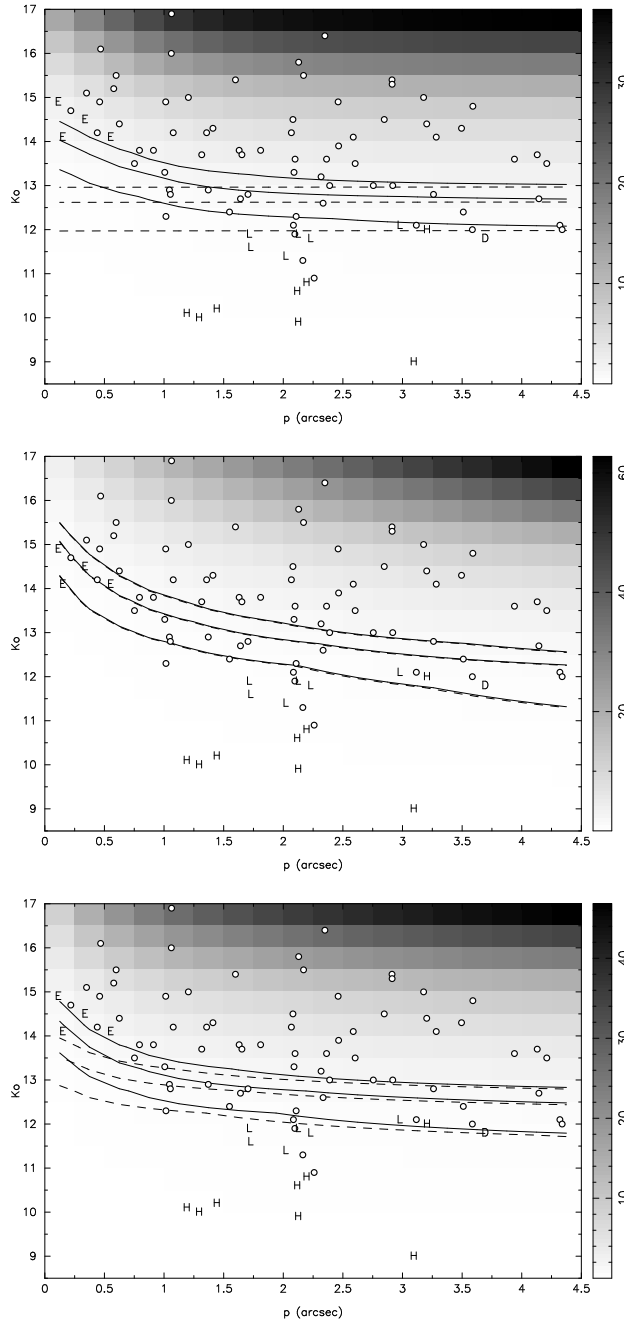


Fig. 9.— The mean number of stars with  $K < K_0$  per  $0.25''$ -wide bin, as expected with collisional destruction of giants (gray-scale and full line contours) and without collisional destruction (dashed line contours). The contour lines mark, from top to bottom, the model predictions for the minimal magnitude below which less than 1.5, 1 and 0.5 stars per  $0.25''$  bin are expected to be observed, on average. Top panel: a  $r^{-2}$  stellar distribution. Middle panel: a flat core in the inner  $10''$  and a  $r^{-2}$  distribution outside. Bottom panel: a  $r^{-3/2}$  distribution in the inner  $10''$  and a  $r^{-2}$  distribution outside. Overlaid on the gray-scale are the stars observed by Ghez et al. (1998), marked by different symbols according to their spectral type (Eckart & Genzel 1997; Genzel et al. 1997): HeI/HI stars (H), late-type stars (L), early-type stars (E), dust embedded stars (D), and type unknown (circle).

Table 1: The Kolmogorov-Smirnov acceptance probabilities for various stellar density models. The broken power-law models have  $r_b = 10''$  and the flattened isothermal model  $r_c = 10''$ . The highest probabilities for each data set are emphasized in italics.

data set	Keck	Keck	OSIRIS	3D+SHARP
Subset	All	old stars	old stars	old stars w/o Sgr A*
No. of stars	64	54	50	107
Flat. isothermal	0.05	0.12	0.41	0.20
$r^{-2}$	0.02	0.02	0.10	0.04
$r^{-7/4}$	0.11	0.12	0.78	<i>0.63</i>
$r^{-3/2}$	<i>0.38</i>	<i>0.37</i>	0.33	0.50
$r^{-7/4} + r^{-2}$	0.09	0.10	0.51	0.34
$r^{-3/2} + r^{-2}$	0.27	0.27	<i>0.91</i>	0.56

Table 2: The frequency of ring-like structures in  $10^7$  Monte-Carlo realizations drawn from a  $n \propto r^{-\alpha}$  density cusp. In each realization, 64 stars are randomly distributed within  $2.5''$ , and the number of rings of width  $\leq 0.06''$  is recorded as function of the number of stars in the ring.

Stars per ring	Rings per realization	Mean ring position
$\alpha = 3/2$		
$\geq 7$	$1.8 \cdot 10^{-1}$	$2.0'' \pm 0.4''$
$\geq 8$	$4.0 \cdot 10^{-2}$	$2.0'' \pm 0.4''$
$\geq 9$	$8.1 \cdot 10^{-3}$	$2.1'' \pm 0.3''$
$\geq 10$	$1.5 \cdot 10^{-3}$	$2.1'' \pm 0.3''$
$\geq 11$	$2.3 \cdot 10^{-4}$	$2.1'' \pm 0.3''$
$\alpha = 2$		
$\geq 7$	$5.4 \cdot 10^{-2}$	$1.3'' \pm 0.7''$
$\geq 8$	$9.2 \cdot 10^{-3}$	$1.3'' \pm 0.7''$
$\geq 9$	$1.4 \cdot 10^{-3}$	$1.3'' \pm 0.7''$
$\geq 10$	$1.9 \cdot 10^{-4}$	$1.3'' \pm 0.7''$
$\geq 11$	$2.3 \cdot 10^{-5}$	$1.3'' \pm 0.7''$

Table 3: The orbital correction factors to the local collisional rate (Eq. B7) and the fraction of unbound stars in the population.

$\alpha$	$\gamma$	$\widehat{C}_g$	$\widehat{C}_f$	$\xi = \alpha + \gamma$	$f_{ub}$
5/2	1	6.2	2.3	7/2	0.07
2	1	3.5	1.7	3	0.11
7/4	1	2.8	1.5	11/4	0.14
3/2	1	2.2	1.4	5/2	0.17
1	1	1.6	1.2	2	0.26
1/2	1	1.1	1.1	3/2	0.39
0	1	0.9	1.0	1	0.57